A Realistic Diffusion Model for Ultrathin Polyelectrolyte Films

Regine v. Klitzing*,† and Helmuth Möhwald‡

Institut für Physikalische Chemie, Universität Mainz, Welder Weg 11, D-55099 Mainz, Germany, and MPI für Kolloid- und Grenzflächenforschung, Rudower Chaussee 5, D-12489 Berlin, Germany

Received February 13, 1996; Revised Manuscript Received July 16, 1996⊗

ABSTRACT: In order to obtain information on transport processes in ultrathin films of polyelectrolytes, we studied the time dependence of the fluorescence of a dye (FITC) attached to a polymer and embedded in a defined, variable depth inside the film by total internal reflection fluorescence (TIRF) spectroscopy. Adding a rhodamine solution to the outer aqueous phase, we observe FITC quenching due to energy transfer and from this determine surface concentration and permeability of rhodamine. We derive a diffusion coefficient on the order of 10^{-15} cm^2/s. This value can be manipulated by changing the film structure. So, the diffusion coefficient varies by nearly 2 orders of magnitude going along the surface normal. Studying the paramagnetic quenching by the smaller spin label TEMPOL, we observe that the diffusion coefficient is more than a factor of 200 larger for this molecule.

I. Introduction

Many applications of ultrathin films require knowledge of the transport of molecules or ions through these films. In the case of films made of polyelectrolytes, this may be a very interesting property since the polymer network may entrap large molecules but be penetrable to small ones. In addition, these films, which can be manufactured with controlled thickness,[1] may yield information on density and dynamics of polymeric films near interfaces.

The films used in the measurements shown in this paper are polyelectrolyte multilayers. They are built up by alternating adsorption of anionic and cationic polyelectrolytes.[2] A special feature of molecular films is that macroscopic properties can be controlled by the microscopic structure.

For permeability measurements a fluorescent dye was embedded in the polyelectrolyte film in defined, variable distances from the surface. The fluorescence was measured after excitation in a TIRF apparatus and was quenched by penetrating molecules of different geometries. Films of different structures were investigated by variation of the polyelectrolyte conformation and by depositing amphiphilic layers into the polyelectrolyte films. A diffusion model is suggested which makes it possible to calculate the diffusion coefficient. The presented measurements give information on the depth dependence of the diffusion coefficient and the size effect of the quencher molecules. The results show an influence of barriers in the film and of the preparation conditions on the transport phenomena as well.

II. Experimental Section

II.1. Materials. Poly(ethylenimine) (PEI, $\bar{M} \sim 55000$), poly(styrenesulfonate sodium salts) (PSS, $\bar{M} \sim 70000$) and poly(allylamine hydrochloride) (PAH, $\bar{M} \sim 57000$) were obtained from Aldrich (Steinheim, Germany). PSS was dialyzed against Milli-Q water and freeze-dried. PEI and PAH were used without further purification. The structural formulas for PAH and PSS are shown in Figure 1a. The dye used was fluorescein isothiocyanate (FITC, Sigma). PAH was labeled with FITC according to the same standard method used for protein labeling.[3] In the following, it is called FITC-PAH. The degree of labeling was about 1 FITC molecule to 400 monomers of PAH. Therefore the influence of the FITC on the deposition process is negligible. If barriers are deposited in the polyelectrolyte film, they are formed by a permanently positively charged amphiphile: dimethyldioctadecylammonium bromide (DODAB, Sigma).

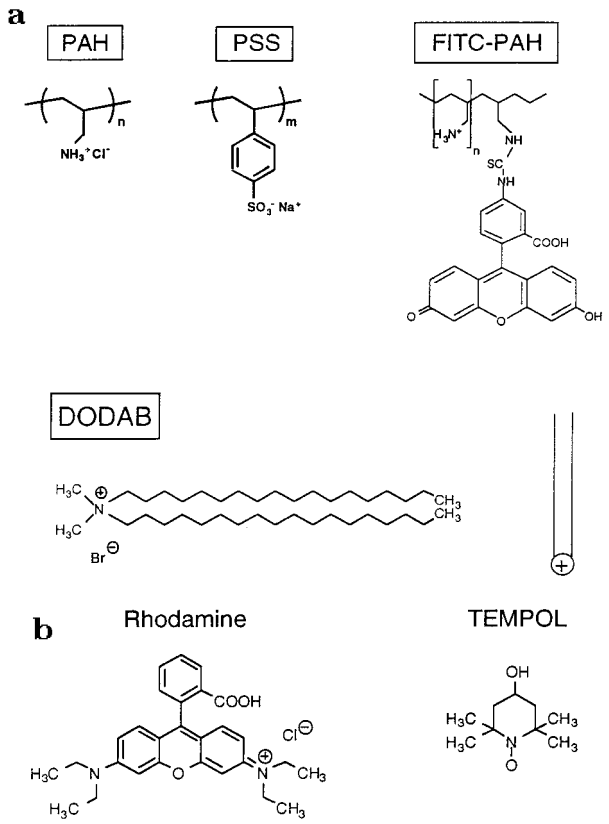

Figure 1. (a) (Top) Polyelectrolytes: the polycation poly(allylamine hydrochloride) (PAH, $n \sim 500-600$), the polyanion poly(styrenesulfonate sodium salt) (PSS, $m \sim 400$), and the FITC-labeled PAH (FITC-PAH) as optical sensor. PEI is not shown here because it is not relevant for the message of this paper. (Bottom) The amphiphile dimethyldioctadecylammonium bromide (DODAB). (b) The quencher molecules rhodamine and TEMPOL.

The quencher molecules rhodamine ($M_R = 479$) and 2,2,6,6-tetramethyl-4-piperidinol 1-oxide (TEMPOL, $M_T = 172.2$) were obtained from Sigma. Their structures are shown in Figure 1b. The aqueous quenching solutions contained 10^{-5} M

* To whom correspondence should be addressed.
† Universität Mainz.
‡ MPI für Kolloid- und Grenzflächenforschung.
⊗ Abstract published in *Advance ACS Abstracts,* September 1, 1996.

S0024-9297(96)00240-9 CCC: $12.00

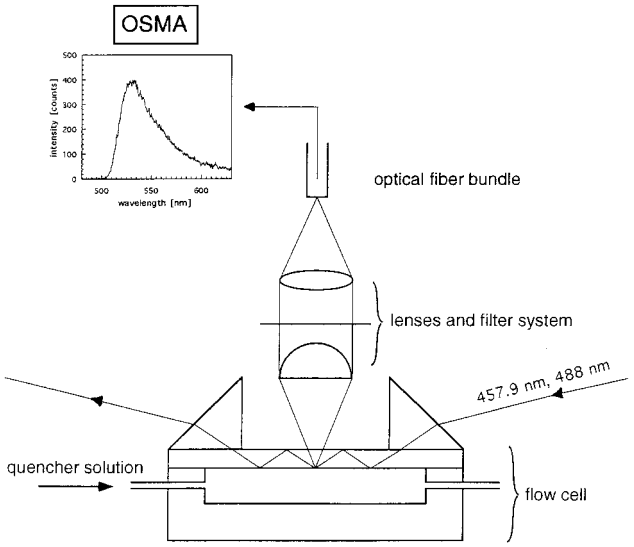

Figure 2. TIRF apparatus including a flow cell to exchange the solution.

rhodamine and 0.1 M TEMPOL, respectively. In order to minimize the inaccuracy due to the pH dependence of the dye fluorescence, all solutions were buffered by a 7×10^{-3} M carbonate buffer of pH = 9.5 where the fluorescein fluorescence is almost independent of the pH value of the environment.

Glass substrates (46 × 13 × 1.3 mm) were purchased from Hellma (Jena, Germany) and cleaned by toluene reflux and plasma cleaner. The substrate served as the top of the flow cell produced by Hellma (Mühlheim, Germany). It consists of a quartz block with two flow channels on the short sides of the cell.

II.2. Apparatus. The TIRF experimental system used is shown in Figure 2 and it is the same as described in ref 4. An argon ion laser beam at 457.9 or 488 nm is coupled into the glass substrate via glass prisms obtained from Spindler & Hoyer (Göttingen, Germany). The coupling angle was fixed at about 70° far away from the critical angle (about 62°). The evanescent field at the substrate surface excited the dye in the polyelectrolyte film on the bottom of the substrate. The fluorescent light was collected through a lens and filter system and an optical fiber bundle, both placed perpendicularly to the substrate at the upper side, and was measured by OSMA (optical simultaneous multichannel analysis). Figure 2 shows a spectrum of the FITC-PAH which was measured in this way.

The substrate with the polyelectrolyte film on its lower side served as the top of the flow cell where different aqueous quencher solutions were flushed in by a pump. The respective film thicknesses were measured by small-angle X-ray scattering (SAXS) via analysis of the so-called Kiessig fringes.[5]

II.3. Film Preparation. The polyelectrolyte films were deposited by immersion for 20 min into aqueous solutions containing 10^{-2} monomol of the respective polyelectrolyte and by dipping in Milli-Q-water for 3 × 1 min after each deposition step. Polyanion and polycation were deposited consecutively via this self-assembly technique.

In order to obtain an increased adsorption, a precursor film with a total thickness of about 140 Å consisting of layers of PEI, PSS, and PAH was deposited on the cleaned substrate. After the last PSS layer, the wafer was coated with FITC-PAH (about 6 Å). Now, different numbers of layers of PSS and PAH were deposited on different substrates (Figure 3a). The thickness of one bilayer PSS/PAH was about 40 Å (thickness PSS:PAH ≈ 2:1) if the polyelectrolyte solutions contained 1.0 mol NaCl and about 8 Å without any additional salt in the polyelectrolyte solutions. The thinnest film has no further PSS or PAH layer on the FITC-PAH layer. The dye is always attached to PAH; hence we compare dye features in identical polyelectrolyte environments. Because of clarity the polyelectrolyte layers are presented without any interdigitation in Figure 3a.

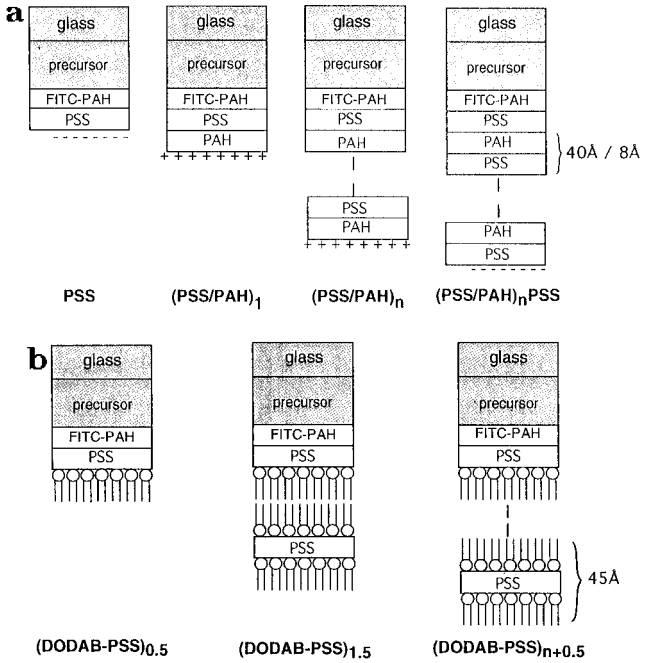

Figure 3. (a) Polyelectrolyte films prepared by consecutive adsorption of polycation (PAH) and polyanion (PSS) from aqueous solutions. Only the structure of the decisive film covering the dye layer (FITC-PAH) is given in detail. (b) Amphiphile/polyelectrolyte films prepared by the LB technique.

For preparing the amphiphile/polyelectrolyte films, the amphiphilic DODAB and the polyanion PSS are deposited via alternating adsorption by the LB technique (Figure 3b). One bilayer has a thickness of about 45 Å.

II.4. Measurement Procedure. Rhodamine and TEMPOL show two different mechanisms of quenching. In the case of rhodamine, energy transfer occurs from fluorescein to rhodamine via dipole−dipole interaction with an interaction radius of about 60 Å (Förster energy transfer). The spin label TEMPOL enhances the spin−orbit coupling in the fluorescein dye with an interaction radius of about 6 Å (paramagnetic quenching). In order to minimize the direct excitation of Rhodamine, the wavelength of the laser light was 457.9 nm. In the experiments with TEMPOL, the FITC was excited by the usual wavelength of 488 nm. The measurements were carried out for different film thicknesses.

The fluorescence intensity was measured up to 300 min after flushing the quencher solution into the cell. The displayed values are integrated fluorescence intensities (515−550 nm for TEMPOL and 520−535 nm for rhodamine experiments) which were normalized with respect to the intensity I_0 for the pure buffer solution without any quencher.

III. Results

Figure 4 shows the fluorescence spectra as a function of time after flushing with rhodamine solution. Obviously, the FITC emission (maximum at 527 nm) decreases simultaneously with an increase of rhodamine fluorescence (maximum at 583 nm). This proves that the FITC fluorescence is really due to energy transfer to the acceptor, and we can use the measurement of this decay to obtain information on the quencher diffusion. The stronger increase of rhodamine fluorescence is caused by additional direct excitation in spite of the low excitation wavelength. Therefore we use the FITC fluorescence decay for a quantitative analysis.

Figure 5a shows the time dependence of the FITC fluorescence intensity for different film thickness up to 480 Å. All measurements show a fluorescence decay with time. With increasing film thickness, the decay

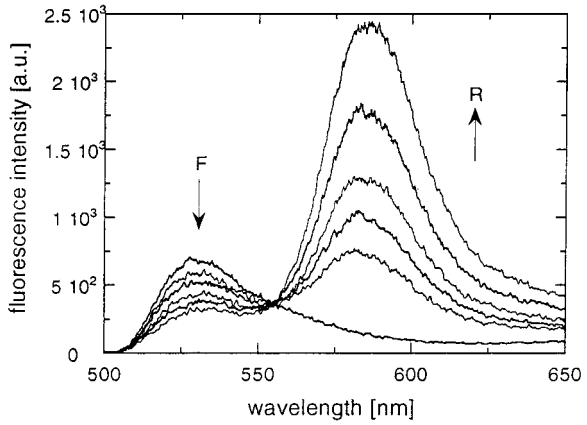

Figure 4. Fluorescence spectra for different times after flushing the rhodamine solution into the cell. The fluorescein dye was embedded in a pure polyelectrolyte film. The arrows are in the direction of increasing time. F = fluorescein fluorescence; R = rhodamine fluorescence.

time increases. The saturation values for films with intermediate film thicknesses are similar (around 43% of the intensity I_0). It could be expected that the data for the thicker films result in a comparable value after measuring a much longer time than 300 min. Yet, the equilibrium values of the films thinner than 80 Å are significantly lower (25−30% of I_0).

The displayed data are for films with PAH at the surface. The results of films with PSS at the surface are similar. They are not shown in this paper.

Until now the polyelectrolyte films were prepared with 1 M NaCl. For investigating the influence of salt concentration during preparation on the transport, some films were also prepared without any additional salt. The number of polyelectrolyte layers was chosen in that way that the film thickness is the same as in the case with 1 M NaCl. The data curves in Figure 5b show shorter decay time than for the films prepared with the high salt concentration.

To get information about the barrier properties of amphiphiles, layers of DODAB were deposited into the polyelectrolyte film. The results presented in Figure 5c show longer decay times than for pure polyelectrolyte films.

In order to obtain information on the dependence of penetration on molecular size, we replaced the quencher rhodamine by the smaller molecule TEMPOL. Figure 5d shows the results for TEMPOL penetrating into films of different thicknesses up to 600 Å. The fluorescence decay is observed as well but the equilibrium data are obtained within the first minutes even for the thickest film. The quenching effect is much smaller than with rhodamine because of different quenching mechanisms. All measurement curves reach similar saturation values of 80−85% of the reference intensity I_0 with the exception of the curve for the film with FITC-PAH at the surface whose equilibrium value is around 65% of I_0.

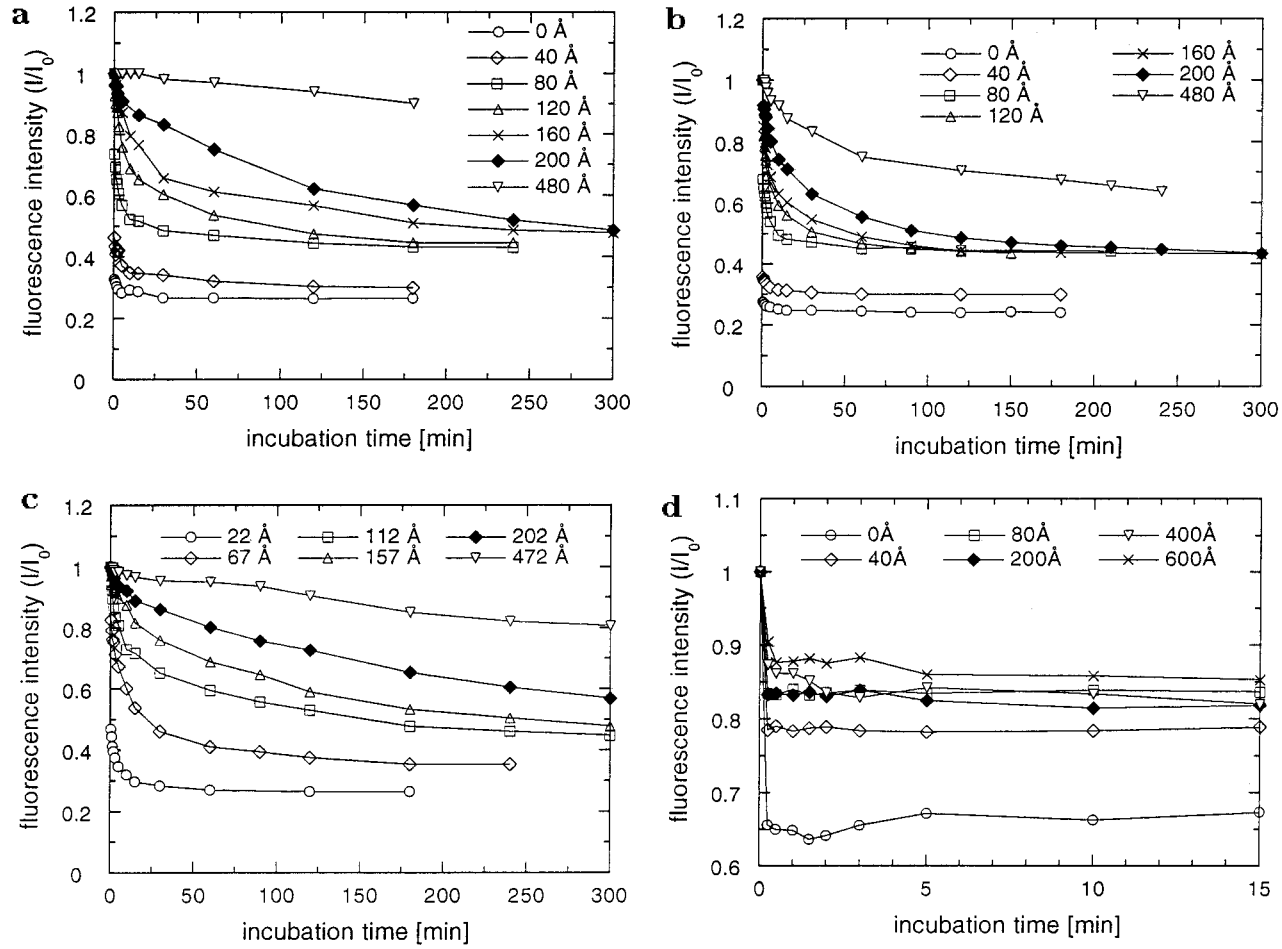

Figure 5. (a) Integrated fluorescence normalized with respect to the intensity without any quencher as a function of time after flushing the rhodamine solution into the cell. The parameter is the thickness of the film on the FITC-PAH layer. Preparation of the covering layers with 1 M NaCl. (b) As in (a), but after salt-free preparation. (c) As in (a), but with an amphiphile/polyelectrolyte film. (d) As in (a), but with TEMPOL as quencher.

IV. Interpretation and Conclusions

Qualitative Aspects. The fluorescence decay proves that polyelectrolyte films are permeable for both rhodamine and TEMPOL molecules.

The quenching of the FITC fluorescence can be divided into contributions from quenchers in two different environments: (i) The molecules in the outer solution quench the dye fluorescence if they approach the dye to establish a distance closer to their interaction radius of 60 Å (for rhodamine) and 6 Å (for TEMPOL), respectively. (ii) The molecules diffusing into the polyelectrolyte film quench the dye fluorescence by the same mechanisms. So, the equilibrium values for intermediate film thicknesses (≥80 Å) correspond to the quencher concentration in the film bulk, and the values for the films with FITC-PAH directly at the surface to the concentration at the surface.

In equilibrium, we assume an approximately uniform distribution of rhodamine molecules in the whole observed film.

The surface charge has no influence on the results presented. This is compatible with the assumption that rhodamine has no net charge in the basic medium. Therefore we would expect that possible weak potential oscillations because of the alternating sequence of polyelectrolytes with positive and negative excess charge have no influence on molecular transport.

The internal film structure, however, has an influence on the transport phenomena. From the ionic strength dependence of the individual layer thickness, we can deduce that at low ionic strength (without any additional salt) the polymers form pancakes at the surface, whereas at high ionic strength (1 M NaCl) they form predominantly loops. The comparison of data measured with films prepared at different ionic strengths then suggests that the transport of rhodamine molecules is about a factor of 3 faster through the flat polyelectrolyte molecules than through the loops. This indicates a less tightly packed structure of films prepared without any additional salt because of a higher electrostatic repulsion between the equally charged polyelectrolytes of one layer. This is confirmed by SAXS data, which show a smaller electron density, and UV−vis measurements, which indicate a smaller polyelectrolyte amount per volume.[6] Another reason for the increased permeability could be that possible defects are more easily smeared out in films with a high salt concentration.

The amphiphiles do not form a complete barrier for the rhodamine molecules but they slow down the transport. The permeability is supposed to be caused by defects of the bilayer film.

The measured intensity curves for films with FITC-PAH directly at the surface show a relative intensity lower than 0.5. So, the concentration of the rhodamine at the surface is slightly above $1/\pi(60\ \text{Å})^2 \approx 1/10000\ \text{Å}^2$. This value corresponds to a few percent of a monolayer.

Quantitative Aspects. For a quantitative analysis, we consider the transport process perpendicular to the film surface (z direction). Because of the uniform quencher distribution in front of the surface ($x-y$ plane) at the start of the measurement the main contribution to the molecular transport is assumed to be given by the one-dimensional diffusion into the film. Fick's second law is[7]

$$\frac{\partial c(z,t)}{\partial t} = D\frac{\partial^2 c(z,t)}{\partial z^2} \tag{1}$$

for the quencher concentration c and the diffusion coefficient D. In comparison with the film, the bulk quencher solution could be considered as infinite. The diffusion coefficient of the molecules is assumed to be higher in the outer aqueous solution ($D \approx 10^{-5}\ \text{cm}^2/\text{s}$)[8] than in the film. So, the bulk solution presents a source which delivers quencher molecules faster to the film−solution interface than the quencher molecules diffuse into the film. Therefore the concentration c_0 at the film surface ($z = 0$) is assumed to be independent of time. So, we consider the diffusion in a semi-infinite medium. The boundary condition ($z = 0$) is

$$c = c_0, \qquad t > 0 \tag{2}$$

and the initial condition ($t = 0$)

$$c = 0, \qquad z > 0 \tag{3}$$

With these conditions, the solution of Fick's second law is[9]

$$c = c_0\ \text{erfc}\left(\frac{z}{2(Dt)^{1/2}}\right) \tag{4}$$

The concentrations were calculated from the measured intensities I/I_0 via the Stern−Volmer relationship. (Investigations where the fluorescence of FITC at the film surface was measured as a function of the outer rhodamine concentration confirmed that the quenching effect $I_0/I - 1$ is proportional to the quencher concentration c). Figure 6a shows the concentration profile for a fixed time of 0.5, 30, and 120 min, respectively, after flushing the rhodamine solution into the cell. It is calculated from the time-dependent intensities in view of the fact that the solution delivers a contribution to the quenching process as well. The measured curves for the two thinnest films presented were adapted in a way that their equilibrium values correspond to the equilibrium values of the curves for intermediate film thicknesses. The profiles confirm the assumption that the concentration at the polyelectrolyte surface is constant during the measurement. The fit of the calculated concentration profiles via eq 4 results in a diffusion coefficient of $D = 8.9 \times 10^{-15}\ \text{cm}^2/\text{s}$ for 0.5 min and $D = 0.15 \times 10^{-15}\ \text{cm}^2/\text{s}$ for 120 min, but this fit is only possible for the top 100 Å. Considering also larger depths, one realizes that the shapes of the profiles are qualitatively different as long as they are described by a single diffusion coefficient. Therefore, we assume that there are two different areas with different diffusion coefficients. Figure 6b shows a simulation according to eq 4 for the same time as in Figure 6a. Up to a 100 Å film depth, the high diffusion coefficient (filled symbols) was used, and from 100 Å on, the lower one (open symbols) was used. The simulation agrees well with the concentration profile above. From this, one can derive the diffusion coefficients, and the values for rhodamine are given in Table 1.

Obviously, in all cases the diffusion coefficient of the first 100 Å is between 1 and 2 orders of magnitude higher than that of the rest of the film. Therefore we deduce that the rhodamine permeability of the layers near the film surface is higher than in the film bulk. This leads us to the conclusion that the outer layers are more loosely packed than the layers far away from the surface in the film bulk. Probably, the loops (and defects) are larger near the surface. This is confirmed by investigations of FITC fluorescence as a function of

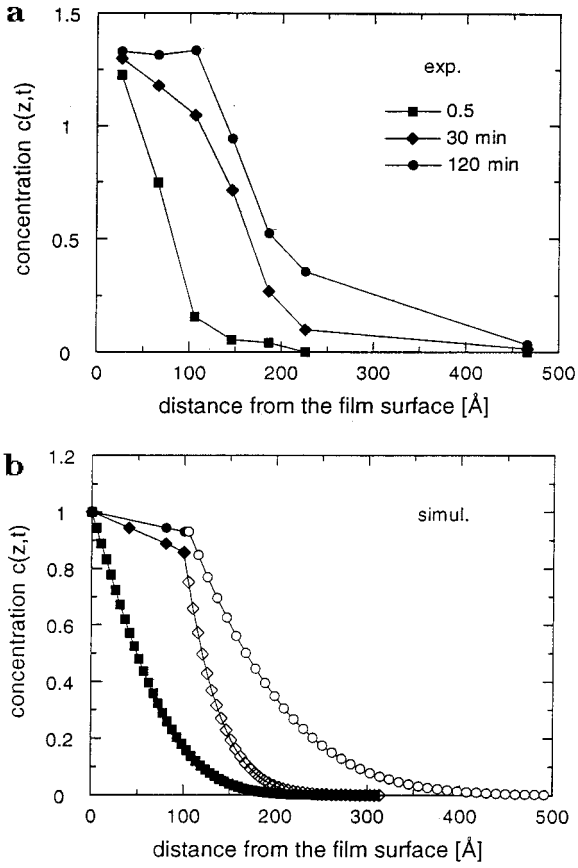

Figure 6. (a) Concentration profile of rhodamine molecules inside the film as a function of the distance from the film surface calculated from the data measured for the polyelectrolyte film of Figure 5a. (b) Simulation of the concentration profile by eq 4 for two different diffusion coefficients: $D = 8.9 \times 10^{-15}$ cm^2/s (filled symbols) up to 100 Å and $D = 0.15 \times 10^{-15}$ cm^2/s (open symbols) from 100 Å on.

Table 1. Diffusion Coefficients (Å^2/s) for Two Different Film Areas

	DODAB	PAH (1 M NaCl)	PSS (1 M NaCl)	PAH (0 M NaCl)
$z \leq 100$ Å	42	99	89	174
$z > 100$ Å	1.0	1.8	1.5	8.6

the dye position in the polyelectrolyte film.[10] The fluorescence decreases by depositing more polyelectrolyte layers on the dye containing layer. This suggests that the quantum yield was reduced in the more solid environment.

The similar diffusion coefficients of the pure polyelectrolyte films and the amphiphile/polyelectrolyte film in the film bulk lead us to the assumption that the structure in both film types is determined by the structure of the polyelectrolytes. Perhaps there is a kind of micellar structure or lamellar crystal in the DODAB layer. Isotherms of DODAB on an aqueous PSS subphase show that in the condensed phase the DODAB molecules are not packed most densely.[11] Only the structure of the outer layers is influenced by the amphiphiles. But the largest effect is obtained by changing the salt concentration during film preparation. Both near the surface and in the film bulk the diffusion coefficient is much higher after adsorption from salt-free solutions.

For TEMPOL, the kinetics cannot be resolved by this method; however, the equilibrium data are quickly obtained. The diffusion coefficient D_T is estimated to be at least 2 orders of magnitude higher than for rhodamine (D_R). From the Stokes−Einstein relationship[12] we get

$$\frac{D_R}{D_T} = \left(\frac{M_T}{M_R}\right)^{1/3} \tag{5}$$

The ratio of masses of TEMPOL M_T and of rhodamine M_R results in a factor of less than 2 in diffusion coefficient in the case that both kinds of molecules experience the same environment (e.g., water). The large difference of diffusion coefficient in the experiments presented here could be explained in that way that the rhodamine molecule can only pass the polyelectrolyte chains by changing its local environment. For TEMPOL the transport could be compared with a transport through cavities formed by the polyelectrolyte chains and filled with water.

Another possible explanation for the lower diffusion coefficient of rhodamine could be an interaction between the local charges of the rhodamine and the charges of the polyelectrolytes in the film, though measurements with the forced Rayleigh scattering technique result in a diffusion coefficient of about 10^{-16} cm^2/s for 2,2′-bis-(4,4-dimethylthiolan-3-one) (TTI) in an electrically neutral polystyrene.[13] TTI has a similar size as the rhodamine molecule and the diffusion coefficients are of the same order. Therefore the Coulomb interaction can be neglected in these studies.

Instead of assuming a depth-dependent transport, the diffusion coefficient could be assumed to be time dependent with decreasing value in time. The physical background would be a dispersive transport. That corresponds to different paths of different transport velocities. For example, the transport would be faster along defects. But in this case the slope of the time-dependent curves (Figure 5a−c) would be depth independent at the beginning of the measurement. In our studies, the slope of the curve depends on the film thickness at every point of time. So we assume a depth-dependent transport.

The fact that the diffusion coefficient of the outer polyelectrolyte layers is almost 2 orders of magnitude higher than that for the film bulk could reflect a gradient of chemical potential inside the film. This could cause a convective flow and therefore the time-dependent concentration profile might not only be due to diffusion. Therefore below we also perform an estimate of possible contributions due to convection.

The flux J of particles is driven by the thermodynamic force F which corresponds to the gradient of the chemical potential $\partial\mu/\partial x$:

$$J = BF = -B\frac{\partial\mu}{\partial x} = -B\frac{\partial\mu^\circ}{\partial x} - \frac{BRT}{c}\left(\frac{\partial c}{\partial x}\right) \tag{6}$$

Therefore the flux of particles is driven by the gradient of the concentration-independent part of the standard chemical potential $\partial\mu^\circ/\partial x$ and by the usual concentration gradient $\partial c/\partial x$ connected with the diffusion coefficient $D = BRT/c$. We consider now the equilibrium state where the flux of particles is zero. The chemical potential for the quencher molecules has to be the same everywhere in the film and in the outer solution. If we consider the potential inside the film bulk (b) and at the surface (s) in equilibrium, we obtain

$$\mu_s^\circ + RT \ln c_s = \mu_b^\circ + RT \ln c_b \tag{7}$$

Because of the Stern−Volmer relationship, it follows

$$\mu_b^\circ - \mu_s^\circ = RT \ln \frac{(I_0/I - 1)_s}{(I_0/I - 1)_b} \quad (8)$$

The fact that the equilibrium intensities for sufficiently thick films ($80 \leq d \leq 140$ Å) deviate by less than 10% also suggests that the variation of the concentration-independent part of the chemical potential is less than 500 J mol^{-1}/60 Å. We thus can now demonstrate that the convective contribution to the flux according to eq 6 is negligible: Inspecting the "short-time" distribution in Figure 6a, we see that the concentration decays by a factor of 10 over a distance of 100 Å. Hence $RT\,\partial \ln c/\partial x \approx 5.7$ kJ mol^{-1}/100 Å. Above, however, we have estimated an upper limit of the concentration independent contribution of $\partial\mu^\circ/\partial x \approx 0.83$ kJ mol^{-1}/100 Å.

Acknowledgment. We thank Johannes Schmitt, Frank Essler, and Gero Decher for helpful discussions and the VW foundation for financial support.

References and Notes

(1) Decher, G.; Schmitt, J. *Prog. Colloid Polym. Sci.* **1992**, *89*, 160.
(2) Decher, G.; Hong, J. D.; Schmitt, J. *Thin Solid Films* **1992**, *210/211*, 381.
(3) Nargessi, R. D.; Smith, D. S. *Methods Enzymol.* **1986**, *122*, 67.
(4) Klitzing, R. v.; Möhwald, H. *Thin Solid Films*, in press.
(5) Kiessig, H. *Ann. Phys.* **1931**, *10*, 769.
(6) Schmitt, J. Dissertation, Mainz University, 1996.
(7) Fick, A. *Ann. Phys.* **1855**, *10*, 59.
(8) Atkins, P. W. *Physical Chemistry*; Oxford University Press: Oxford, 1987.
(9) Crank, J. *The Mathematics of Diffusion*, 2nd ed.; Oxford Science Publication: Oxford, 1987.
(10) Klitzing, R. v.; Möhwald, H. *Langmuir* **1995**, *11*, 3554.
(11) Essler, F. Diploma thesis, Mainz University, 1992.
(12) Einstein, A. *Ann. Phys.* **1905**, *17*, 549.
(13) Ehlich, D.; Sillescu, H. *Macromolecules* **1990**, *23*, 1600.

MA960240S